[논 문] 한국재료학회지
Korean J. Mater. Res.
Vol. 33, No. 12 (2023)
https://doi.org/10.3740/MRSK.2023.33.12.503

Enhancing Thermal Conductivity in Epoxy Composites with Functionalized Boron Nitride Nanosheets

Yang Soo Kim[1], Ik-Tae Im[2], and Jong Seok Kim[3†]

[1]Korea Basic Science Institute, Jeonju 54896, Republic of Korea
[2]Department of Mechanical Design Engineering, Jeonbuk National University, Jeonju 54896, Republic of Korea
[3]School of Chemical Engineering, Jeonbuk National University, Jeonju 54896, Republic of Korea

(Received October 26, 2023 : Revised November 21, 2023 : Accepted November 21, 2023)

Abstract This comprehensive study delves into the intricate process of exfoliating and functionalizing boron nitride nanosheets (BNNSs) extracted from hexagonal boron nitride (h-BN), and meticulously explores their potential application within epoxy composites. The extensive research methodology encompasses a sequence of treatments involving hydrothermal and sonication processes aimed at augmenting the dispersion of BNNSs in solvents. Leveraging advanced analytical techniques such as Raman spectroscopy, X-ray diffraction, and FTIR spectroscopy, the study rigorously analyzes a spectrum of changes in the BNNS's properties, including layer count variations, interlayer interactions, crystal structure modifications, and the introduction of functional groups. The research also rigorously evaluates the impact of integrating BNNSs, specifically glycidyl methacrylate (GMA)-functionalized BNNSs, on the thermal conductivity of epoxy composites. The conclusive findings exhibit notable enhancements in thermal properties, predominantly attributed to the enhanced dispersion of fillers and enhanced interactions within the epoxy matrix. This pioneering work illuminates the wide potential of functionalized BNNSs for significantly enhancing the thermal conductivity of epoxy composites, paving the way for advanced materials engineering and practical applications.

Key words boron nitride nanosheets, exfoliation, functionalization, epoxy composites, thermal conductivity.

1. Introduction

In recent years, rapid industrialization and device development have led to the need for portability, lightweight, and high functionality in many areas, such as automotive components, PCs, home appliances, mobile phones, portable devices, and light-emitting diodes.[1,2] As devices become more densely packed, the heat density inside electronic devices increases. If the heat is not effectively dissipated, it can cause many problems, such as reduced durability, malfunction, explosion risk, reduced lifespan, and discoloration of the device.[3,4] Therefore, developing heat-dissipation materials is essential for electronic devices. Metals with high thermal conductivity have been used for heat-dissipation materials. Still, due to their increased weight and low formability, they are unsuitable for ultra-small electronic devices requiring light, so many studies have been conducted to replace metals.[5,6]

In the case of thermosetting resins, they have good adhesion properties, but their low thermal conductivity makes them challenging to use as heat-dissipation materials. Therefore, many studies have been conducted to compensate for the shortcomings of metals by using composite materials with high thermal conductivity fillers, such as carbon and ceramic materials.[7] Until now, researchers have mixed with high thermal conductivity such as aluminum nitride (AlN), alumina (Al_2O_3), silicon carbide (SiC), magnesium oxide (MgO), and graphene to increase the thermal conductivity of

†Corresponding author
E-Mail : js-kim@jbnu.ac.kr (J. S. Kim, Jeonbuk Nat'l Univ.)

the polymer matrix.[8-12] Carbon-based materials such as graphene, carbon nanotubes, and fullerenes have been used as fillers for optical devices and heat-dissipation materials.[13] Unlike other fields, electrical insulation materials and heat dissipation require high voltage withstand capability along with electrical insulation. Hexagonal boron nitride (h-BNs) can be exfoliated into 2D boron nitride nanosheets (BNNSs), and the thermal conductivity is higher in the horizontal direction. BNNS from h-BN has excellent heat dissipation and electrical insulation properties as a filler and epoxy resin as a matrix.[14] Besides their high thermal stability, they are corrosion-resistant to acids and alkalis.[15] The hydrothermal reaction process, combined with sonication in a solution of h-BN, produces OH-BNNS, enhancing the contact between the matrix and the filler to improve dispersibility.[16,17]

The high filler contents with enormous thermal conductivity are a significant part of improving thermal conductivity because they increase the heat transfer path between the filler and the filler.[18] However, as the filler has huge content, the viscosity of the composites rapidly increases. This results in difficult processing conditions and the deterioration of mechanical properties. In addition, a large amount of filler increases the heat loss due to the higher thermal resistance between the filler and the matrix. It causes low dispersion, a factor that reduces the thermal conductivity.[19] Therefore, much research has been conducted to reduce the contact resistance between the matrix and BNNS by functionalization and surface modification to produce composites with high thermal conductivity and low content by inducing high dispersion.[20-22]

Herein, we report a novel strategy for the fabrication of BNNS by hydrothermal reaction, and ultrasonic exfoliation was performed in a polarized solution because it was thought that the layered structure of BNNS could be peeled off through ultrasonic waves. Enhancing the surface adhesion and dispersion of BNNS with epoxy resins was achieved by polymerization involving glycidyl methacrylate (GMA). Highly thermally conductive composites were prepared by impregnating epoxy resin into the BNNS. A high thermal conductivity of 3.4 W/m · K was achieved at 20 wt% BNNS loading level, corresponding to a thermal conductivity enhancement of about 1,600 %. The notable enhancement observed can be credited to the effective distribution of the additive material and subsequent interactions between GMA and OH-BNNSs. These interactions led to decreased thermal contact resistance and the formation of more efficient pathways for heat transfer. The composites exhibit strong potential for thermal management applications for various technological needs, particularly electronic packaging.

2. Experimental Procedure

2.1. Materials

The epoxy resin based on diglycidyl ether of bisphenol A (YD-128) and the modified aliphatic amine (KH-602) hardener were purchased from Kukdo Chem. Co., Korea. Hexagonal boron nitride (h-BN) powder (average diameter 5 μm, 98 %) was purchased from M. K. Impex Co. Ltd., Canada. Isopropyl alcohol (IPA, 99.9 %), N-methyl-2-pyrrolidone (NMP, 99.7 %), glycidyl methacrylate (GMA, 98 %), azobisisobutyronitrile (AIBN, 99 %), and deionized water (DI water, HPLC grade) were obtained from Daejung Chemicals Co. Ltd., Korea. These chemicals were used as received without any further treatment.

2.2. Preparation of BN nanosheet (BNNS) and functionalization of BNNS (GMA-BNNS)

To exfoliation of h-BN, 500 mg h-BN powders and 100 mL 30 % IPA solution were sonicated at room temperature (RT) for 30 min in an ultrasonic bath (WUC-D03H, 290 W). The h-BN solution was transferred to a 150 mL Teflon-lined stainless steel hydrothermal reactor. Then, the reactor was maintained at 200 °C for 12 h. After hydrothermal reaction, the h-BN solution was fed into a flat-bottomed beaker and was sonicated for 3 h using Sonics VCX 750 (Sonics & Materials, INC., USA) operating at 20 kHz frequency with a power rating of 750 W. After an hour of stillness, the h-BN solution was kept at RT. Finally, after centrifugation (1,500 rpm/min), the sample was washed and dried at 80 °C overnight. The hydroxyl-functionalized BN nanosheets (OH-BNNSs) obtained by sonication and thermal-assisted hydrolysis exhibited high stability in IPA and water mixed solution due to the hydroxylation of BNNSs.

The pH of the reaction mixture was adjusted to 4 using 5 M acetic acid. 500 mg of OH-BNNS and 0.1 mL of GMA ultrasonically dispersed for 30 min in NMP solution in a 250 mL round-bottom flask. The solution was stirred under a

nitrogen atmosphere, 3 mg of AIBN was added, and the reaction was continued at 70 °C for 24 h. PGMA grafted OH-BNNS (GMA-BNNS) was prepared by radical polymerization of GMA. GMA-BNNS vacuum filtered using 0.2 μm polyvinylidene fluoride (PVDF) membrane washed with ethanol and dried at 80 °C overnight.

2.3. Preparation of epoxy nanocomposite

To fabricate the epoxy composite, initially, h-BN, OH-BNNS, and GMA-BNNS fillers were dispersed into ethanol with 5, 10, 15, and 20 wt% via sonication for 30 minutes and added in a definite amount of epoxy. The mixture was heated at 60 °C for 15 minutes to evaporate the ethanol and shear mixed in a Thinky mixer (ARE-310) at 1,000 RPM, followed by sonication at ambient temperature for 10 min. The curing agent (KH-602) is added to epoxy resin with 100:25 (epoxy: curing agent). The epoxy resin, SM-BNNS, and KH-602 mixtures were mechanically mixed and then sonicated at room temperature for 30 min. The prepared composite was degassed to eliminate the trapped air bubbles and finally cast into a Teflon mold.

2.4. Characterization

Surface modification of filler is characterized by Fourier transform infrared spectrophotometer (FT/IR-4100, JASCO, Japan). Raman scattering was performed on a Raman confocal spectroscopy (Nanofinder®, Tokyo Instruments Inc., Japan). The crystal structure of h-BN, BNNS, and GMA-BN NSs was analyzed by X-ray Diffraction (X'Pert Pro Powder, PANalytical, Netherland). The TEM Images were recorded by high-resolution transmission electron microscopy (JEOL 2200 FS, JEOL Ltd., USA) operating at 200 kV. The surface morphology and elemental analysis were observed on field emission scanning electron microscopy (FE-SEM) (Carl Zeiss Supra 40VP, Carl Zeiss AG, Germany). The in-plane thermal conductivity of epoxy thin film (sample dimension: 30 mm × 5 mm × 0.3 mm) was characterized by thermal diffusivity analyzer ULVAC LPIT (Laser-PIT-M2, ULVAC Inc., Japan) at room temperature. Thermal stability parameters were measured using a thermogravimetric analyzer (TGA-Q50, TA Instruments, USA).

3. Results and Discussion

Fig. 1 is a schematic diagram of the interactive exfoliation and functionalization process of OH-BNNS from the h-BN. In the hypothesis, the hydrothermal reaction process of h-BN at high temperatures can enlarge the distance between the adjacent h-BN layers, resulting in an expanded structure. Subsequently, sonication treatment of h-BN could introduce hydroxyl groups on its surface, improving the dispersion of h-BN in solvents. The reason why the hydroxyl (OH) group can be introduced successfully onto the BNNS surface by sonication treatment is as follows. The hydroxyl molecules in the water were excited during the hydrothermal reaction and sonication. When used in sonication conditions, water was discovered to be a successful agent for exfoliating and dispersing h-BN, resulting in pristine h-BN nanosheet dispersions.[23] The exfoliation process was attributed to the influence of solvent polarity and the assistance of sonication-induced hydrolysis of h-BN. Through the sonication process, a powerful longitudinal shear force is employed, resulting in the thorough exfoliation of the bulk h-BN into BNNSs characterized by a minimal layer count and reduced lateral dimensions. The presence of attached OH groups further distinguishes these BNNSs.

Raman spectroscopy was conducted using a 514.5 nm wavelength laser source. Fig. 2(a) displays the Raman spectra of exfoliated BNNSs as sonication time. In the case of bulk h-BN, a strong peak at 1,365 cm^{-1} corresponds to the high-frequency interlayer Raman active E_{2g} stretching mode of BN,[24] the ability of Raman signals to assess interlayer interactions. However, following exfoliation, the Raman active E_{2g} mode of exfoliated BNNS for 1 h sonication time is observed at a slightly lower wavelength (1,366.8 cm^{-1}) and with reduced intensity, indicating a decrease in the number

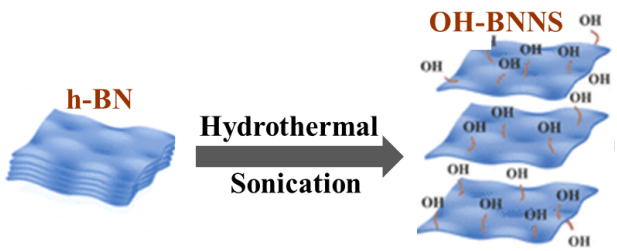

Fig. 1. Schematic illustration of the exfoliation and functionalization process for OH-BNNS.

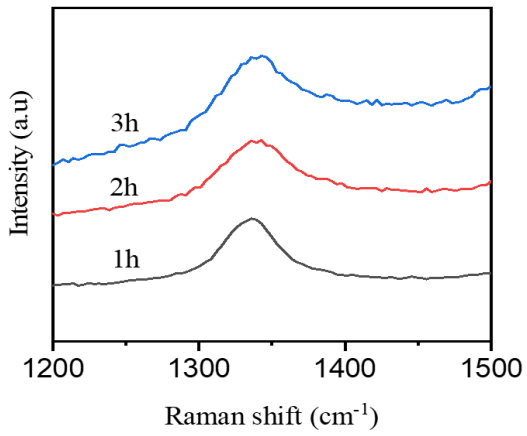

Fig. 2. Raman spectra of OH-BNNs in different sonication times.

of layers. The characteristic peaks of BNNS exfoliated for 2 h and 3 h sonication time were 1,370.7 cm^{-1} and 1,371.7 cm^{-1}. This shift is attributed to a weaker interlayer interaction within the exfoliated BNNS, which has lower mass density and more defect states.

X-ray diffraction (XRD) is employed to analyze the crystal structure and phase composition. Fig. 3(a) displays the XRD profiles for h-BN and GMA-BNNS. The hexagonal phase of h-BN, represented by peaks at 2θ = 26.73°, 41.5°, 43.7°, 50.14°, 55.13°, 71.32°, corresponds to the (002), (100), (101), (102), (004), (103), (104) crystallographic planes, respectively, as per the JCPDS card no. 73-2095. In contrast, these peaks exhibit reduced intensity in the XRD pattern of GMA-BNNS. Additionally, the primary peak (002) of OH-BNNS indicates a decrease in intensity due to a change in density during the exfoliation process.

FTIR spectra of h-BN, OH-BNNSs (3 h sonication time), and GMA-BNNS are shown in Fig. 3(b). The peaks of h-BN were identified at 1,365 and 796 cm^{-1}, associated with B-N in-plane stretching vibration mode and B-N-B out-of-plane bending vibration mode. After hydrothermal reaction and sonication, not only a hydroxyl (OH) peak of OH-BNNS was found at 3,350~3,500 cm^{-1}, but also the BN-O peak at 1,120 cm^{-1} was superimposed due to the broad region present in the region O-B-N. GMA-BNNS. OH-BNNS surface modified with GMA, the C-H peak of GMA-BNNs at 2,843~3,000 cm^{-1} were identified.

Fig. 4 shows the exfoliated filler's phase image as a time function. SEM images confirmed the sample preparation after dispersing the h-BNs and OH-BNNSs (1, 2, and 3 h sonication time). The average particle size of h-BNs is about 5.1 μm. In exfoliated boron nitride nanosheets, by applying ultrasonic energy for 1 h after hydrothermal reaction, the particles are generally distributed with particles larger than 4.5 μm. The average particle size in OH-BNNSs for 2 h sonication time was 4 μm. Its particle size is smaller than OH-BNNSs for 1 h sonication time. The particle size in 3 h sonication time was further reduced compared to 2 h sonication time, and the average particle size was 3.6 μm. When h-BNs were exfoliated by hydrothermal reaction and sonication using IPA/water mixed polar solvent, the thickness of and particle size OH-BNNSs were reduced due to the cutting phenomenon of the particles in addition to the exfoliation of OH-BNNSs.[25)]

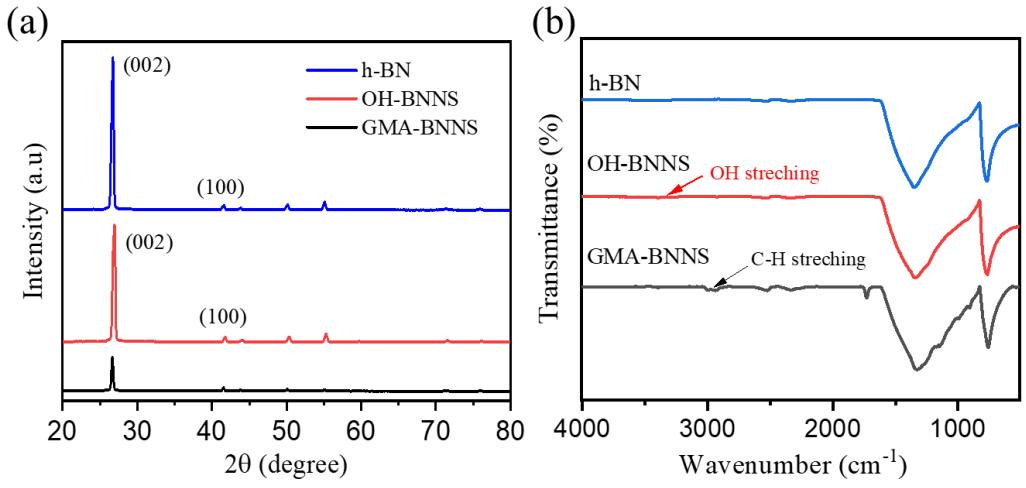

Fig. 3. (a) XRD spectra of h-BN, OH-BNNS, and GMA-BNNS, (b) Fourier transform infrared (FTIR) spectra of h-BN, OH-BNNS, and GMA-BNNS.

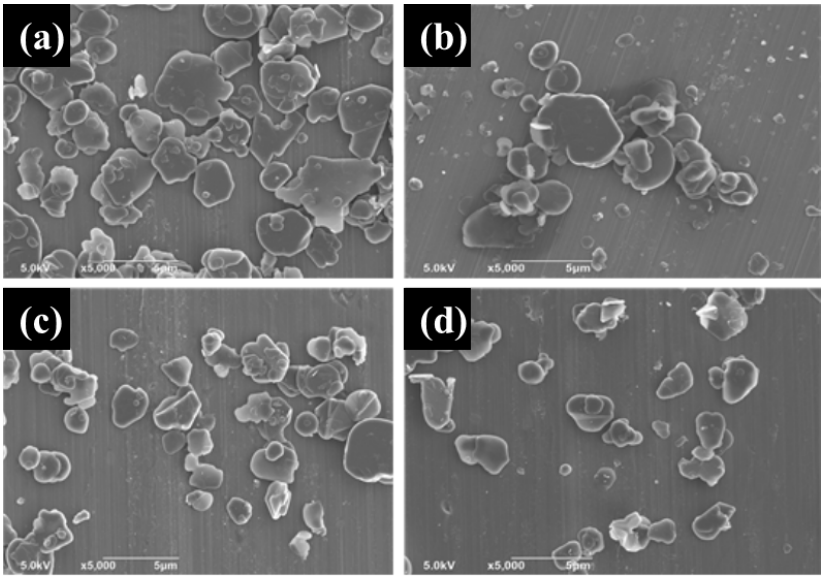

Fig. 4. Scanning electron microscopy (SEM) images of (a) h-BN, (b-d) OH-BNNS in different sonication times, (b) 1 h, (c) 2 h, (d) 3 h.

The shape, size, and structure of exfoliated OH-BNNSs (1 h and 3 h sonication time) in TEM images are shown in Fig. 5. The BNNS peeled off for 1 h have many nanosheets superimposed in the center. The stacking phenomenon of OH-BNNSs can be seen in Fig. 5(c), where more than 20 layers can be seen. The stacking phenomenon of h-BNNs after 3 h sonication time can be seen in Fig. 5(d), with about 10 layers. The number of layers of OH-BNNSs decreases with the ultrasonic exfoliation time. Although sonication of h-BNs breaks the van der Waals bonds, it maintains the strong covalent bonds, resulting in h-BNNs with a few layered structures with a separated morphology between the layers of OH-BNNSs. In this process, it is unfeasible to observe a singular layer of OH-BNNSs, and achieving complete exfoliation leads to exceedingly low yields, thereby presenting a formidable obstacle when attempting to utilize only a few layers of OH-BNNS.

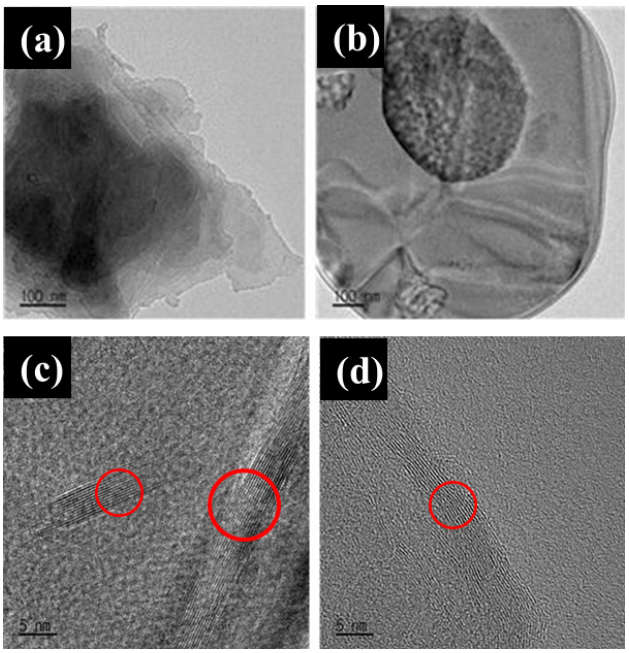

Fig. 5. TEM images of OH-BNNS at sonication times, (a) 1 h and (b) 3 h.

The TGA curve of pure h-BNs and the polymerized GMA (PGMA) coated on the OH-BNNS (GMA-BNNS) is shown in Fig. 6. The analysis was carried out from room temperature to 800 °C and measured at a 20 °C/min ramp rate in a nitrogen atmosphere. In the case of h-BN, the mass was 99.4

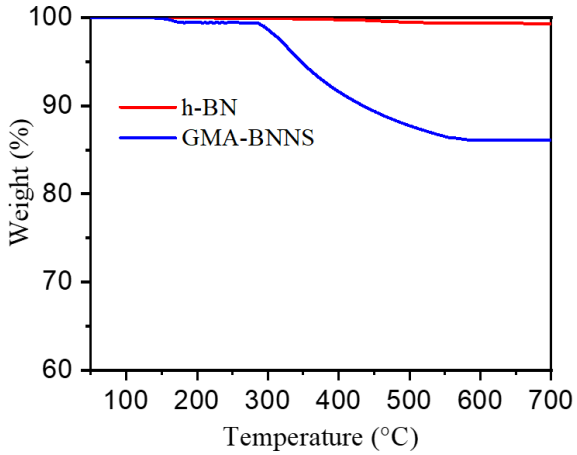

Fig. 6. TGA curves of h-BN and GMA-BNNS.

wt% at 800 °C with a mass loss of 0.6 wt%. Since h-BN is a very thermally stable material, little thermal degradation was observed. The GMA-BNNS started to lose mass rapidly at around 250 °C, with most thermal degradation occurring at 500 °C. As a result, at 800 °C, GMA-BNNS showed a mass loss of 14.8 wt%. The cause of the mass loss of GMA-BNNS seems to be the effect of PGMA.

SEM images of fracture surface in an epoxy matrix, 20 wt% filler of h-BNs/epoxy, OH-BNNSs/epoxy, and GMA-BNNSs/epoxy nanocomposites are shown in Fig. 7. To compare the effect of OH-BNNSs and GMA-modified BNNSs on the dispersibility in epoxy nanocomposites. Fig. 7(a) shows the morphology of the fractured surface of the epoxy matrix after being immersed in liquid nitrogen. The h-BN/epoxy composite in Fig. 7(b) indicates that the h-BN particles agglomerate and show a flat fracture surface due to epoxy matrix without interaction between filler and epoxy matrix. OH-BNNSs and GMA-BNNSs are evenly distributed throughout epoxy nanocomposites in Fig. 7(c, d), indicating high dispersibility. In the case of GMA-BNNSs/epoxy nanocomposite in Fig. 7(d), it can be seen that the rough surface of the nanocomposites is uniformly distributed as the interface reaction between the epoxy matrix and filler with the epoxide group.[26)]

Fig. 8 illustrates how the functionalization of Boron nitride nanosheets (BNNSs) affects the in-plane thermal conductivity of epoxy composites. The thermal conductivity increases as the thermally conductive filler content increases. Specifically, the GMA-BNNS/epoxy composite exhibits superior thermal conductivity to OH-BNNS/epoxy and pure epoxy matrix. In comparison to the baseline, which is neat epoxy with a thermal conductivity of 0.2 $Wm^{-1} K^{-1}$, the in-plane thermal conductivity of h-BN/epoxy improves gradually as the h-BN content increases, reaching a maximum thermal conductivity of approximately 1.11 $Wm^{-1} K^{-1}$, as depicted in Fig. 8(a).

The OH-BNNS/epoxy composite, with 20 wt% OH-BN NS filler, surpasses h-BN/epoxy with an impressive thermal conductivity of about 2.47 $Wm^{-1} K^{-1}$, marking a remarkable increase of approximately 223 % over h-BN/epoxy. The thermal conductivity of OH-BNNS/epoxy experiences a linear rise with increasing filler content, but it shares a significant upturn after reaching 15 wt% OH-BNNs/Epoxy. This boost can be attributed to the higher filler concentration, which leads to a more interconnected network within the composite. The thermal conductivity eventually reaches 3.40 Wm^{-1}

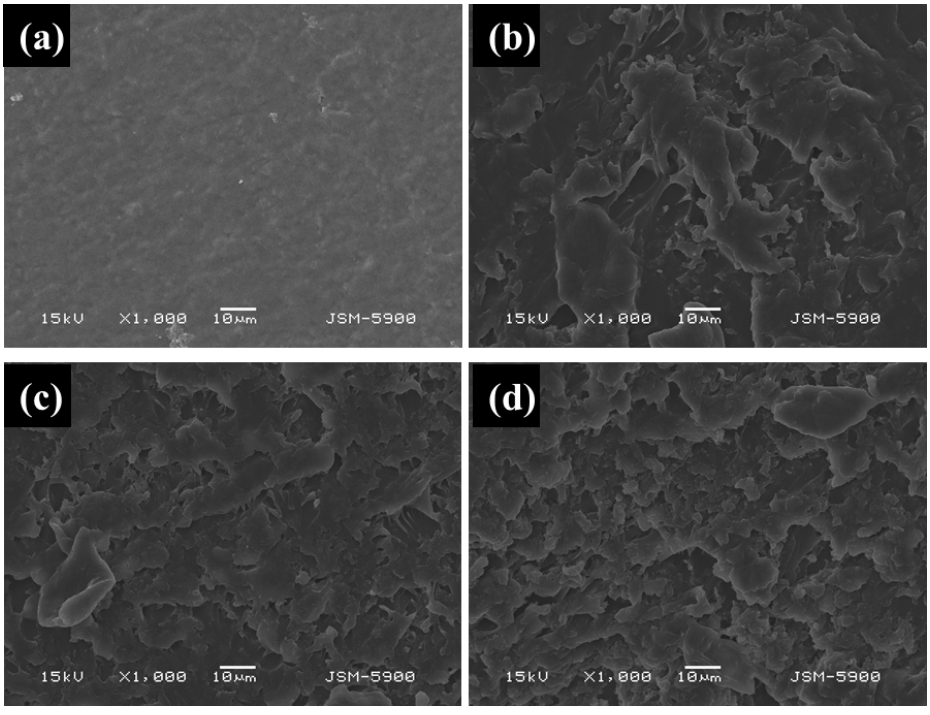

Fig. 7. SEM images of a fracture surface of epoxy nanocomposites with 20 wt% of (a) neat epoxy, (b) h-BN, (c) OH-BNNS, and (d) GMA-BNNS.

K^{-1} in the in-plane direction when 20 wt% of GMA-BNNS filler is incorporated into the epoxy. This value is significantly higher than that of h-BN/epoxy and OH-BNNs/epoxy, resulting in a notable enhancement factor (EF) of approximately 16 concerning neat epoxy, as depicted in Fig. 8(b). The EF represents a thermal conductivity ratio, indicating the degree of enhancement in the thermal conductivity of neat epoxy compared to that of h-BN/epoxy, OH-BNNs/epoxy, and GMA-BNNs/epoxy nanocomposites.

The improvement in thermal conductivity can be attributed to the uniform dispersion of the filler and the interactions between GMA and OH-BNNS after graft polymerization on the BNNS surface. The surface modification of the filler powerfully contributes to forming a robust interface between GMA-BNNS and the epoxy matrix, thereby promoting better dispersion of filler dispersion within the polymer matrix.[11] This, in turn, reduces thermal contact resistance at junctions, leading to more effective pathways for thermal conduction and an overall improvement in thermal conductivity.

4. Conclusion

This comprehensive study has successfully demonstrated the efficacy of exfoliating and functionalizing boron nitride nanosheets (BNNSs) derived from hexagonal boron nitride (h-BN), showcasing their substantial influence on the properties of epoxy composites. BNNSs were effectively tailored to enhance their solubility through a meticulously executed sequence of treatments, leading to significant alterations in their structural and chemical characteristics. Raman spectroscopy revealed a notable reduction in layer count and interlayer interactions, while X-ray diffraction unveiled modifications in crystal structure and interlayer spacing. Additionally, the introduction of functional groups was unequivocally confirmed through FTIR spectroscopy.

Moreover, this research systematically investigated the thermal behavior of these functionally enhanced BNNSs when incorporated into epoxy composites. The results unequivocally demonstrated a substantial enhancement in thermal conductivity, particularly in the context of GMA-BN NSs, compared to pure epoxy's baseline characteristics. This significant improvement can be attributed to the efficient dispersion of the filler and the ensuing interactions between the GMA and OH-BNNSs, which resulted in a reduction in thermal contact resistance and the establishment of more effective thermal pathways. These findings underscore the substantial potential of functionalized BNNSs as a promising additive for elevating the thermal properties of epoxy composites, thereby opening new avenues for developing advanced materials with markedly improved thermal conductivity. These advancements hold considerable promise for various applications across diverse industries.

Acknowledgement

This work was supported by the Jeonbuk National University research fund for 2022.

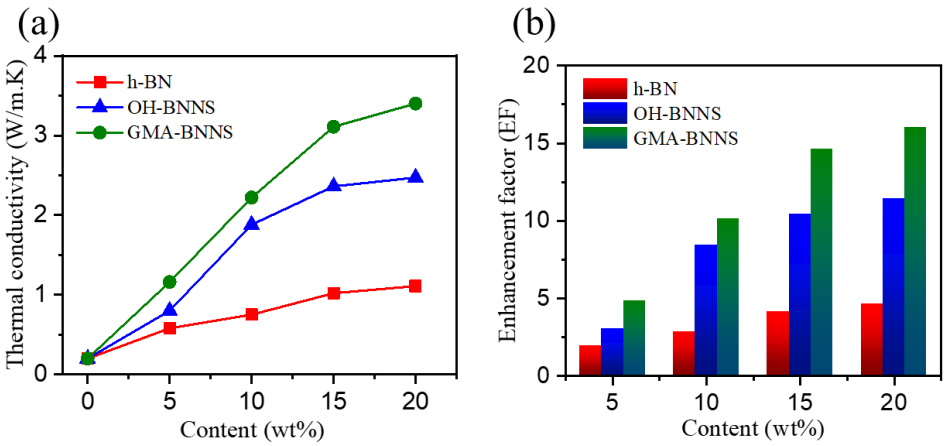

Fig. 8. Thermal conductive properties of neat epoxy and its nanocomposites: (a) thermal conductivity of epoxy, h-BN, OH-BNNS, and GMA-BNNS and (b) thermal conductivity enhancement as a function of filler content.

References

1. L. Zaheed and R. J. J. Jachuck, Appl. Therm. Eng., **24**, 2323 (2004).
2. R. Liu, D. Schreurs, W. De Raedt, F. Vanaverbeke, R. Mertens and I. De Wolf, Microelectron. Reliab., **51**, 1788 (2011).
3. P. Murugapandiyan, D. Nirmal, M. Tanvir Hasan, A. Varghese, J. Ajayan, A. S. Augustine Fletcher and N. Ramkumar, Mater. Sci. Eng., B, **73**, 115449 (2021).
4. L. X. Luo, R. Hu, S. Liu and K. Wang, Prog. Energy Combust. Sci., **56**, 1 (2016).
5. P. Zhang, P. Yuan, X. Jiang, S. Zhai, J. Zeng, Y. Xian, H. Qin and D. Yang, Small, **14**, 1702769 (2018).
6. H. E. Lee, D. Lee, T. Lee, J. H. Shin, G. Cho, C. Kim, S. H. Lee, J. H. Lee, Y. H. Kim, S. Kang, S. H. Park, I. Kang, T. Kim, B. Bae and K. J. Lee, Nano Energy, **55**, 454 (2019).
7. G. Hetsroni, A. Mosyak, Z. Segal and G. Ziskind, Int. J. Heat Mass Transfer, **45**, 3275 (2002).
8. R. S. Prasher, J. Y. Chang, I. Sauciuc, S. Narasimhan, D. Chau, G. Chrysler, A. Myers, S. Prstic and C. Hu, Intel Technol. J., **9**, 285 (2005).
9. W. Zhou, S. Qi, Q. An, H. Zhao and N. Liu, Mater. Res. Bull., **42**, 1863 (2007).
10. M. W. Akhtar, Y. S. Lee, C. M. Yang and J. S. Kim, RSC Adv., **102**, 100448 (2016).
11. M. W. Akhtar, Y. S. Lee, D. J. Yoo and J. S. Kim, Composites, Part B, **131**, 184 (2017).
12. M. W. Akhtar, J. S. Kim, M. A. Memom, M. T. Khan and M. M. Baloch, J. Mater. Sci.: Mater. Electron., **32**, 15307 (2021).
13. Z. Han and A. Fina, Prog. Polym. Sci., **36**, 914 (2011).
14. W. Zhou, S. Qi, Q. An, H. Zhao and N. Liu, Mater. Res. Bull., **42**, 1863 (2007).
15. V. Guerra, C. Wan and T. McNally, Prog. Mater. Sci., **100**, 170 (2019).
16. J. H. Warner, M. H. Rummeli, A. Bachmatiuk and B. Buchner, ACS Nano, **4**, 1299 (2010).
17. K. L. Marsh, M. Soulimana and R. B. Kaner, Chem. Commun., **51**, 187 (2015).
18. S. Wanga, R. Liang, B. Wang and C. Zhang, Carbon, **47**, 53 (2009).
19. K. Kim, M. Kim, Y. Hwang and J. H. Kim, Ceram. Int., **40**, 2047 (2014).
20. K. Kim, H. Ju and J. H. Kim, Compos. Sci. Technol., **123**, 99 (2016).
21. J. Lee and J. H. Kim, Compos. Commun., **28**, 100935 (2021).
22. S. Bayir, E. Semerci and T. E. Bedri, Composites, Part B, **146**, 106406 (2021).
23. Y. Lin, T. V. Williams, T. Xu, W. Cao, H. E. Elsayed-Ali and J. W. Connell, J. Phys. Chem. C, **115**, 2679 (2011).
24. T. Sainsbury, A. Satti, P. May, Z. Wang, I. McGovern, Y. K. Gun'ko and J. Coleman, J. Am. Chem. Soc., **134**, 18758 (2012).
25. S. Zhao, L. S. Schadler, R. Duncan, H. Hillborg and T. Auletta, Compos. Sci. Technol., **68**, 2965 (2008).
26. T. Jiang, T. Kuila, N. H. Kim, B. C. Ku and J. H. Lee, Compos. Sci. Technol., **79**, 115 (2013).

Author Information

Yang Soo Kim

Principal Researcher, Korea Basic Science Institute

Ik-Tae Im

Professor, Department of Mechanical Design Engineering, Jeonbuk National University

Jong Seok Kim

Professor, School of Chemical Engineering, Jeonbuk National University